Journal of Materials Chemistry A

Accepted Manuscript

ROYAL SOCIETY OF CHEMISTRY

www.rsc.org/materialsA

Journal Name

ARTICLE

Cooperative Assembly of Active Layer Utilizing the Synergistic Effect of Functional Fullerene Triad as Acceptor for Efficient P3HT-based Polymer Solar Cells

Received 00th January 20xx,
Accepted 00th January 20xx

DOI: 10.1039/x0xx00000x

www.rsc.org/

Yue Zhao,[a] Guiying Xu,[a] Xia Guo,[a] Yijun Xia,[a] Chaohua Cui,[a] Maojie Zhang,[a] Bo Song,[a] Yaowen Li,*[a] Yongfang Li*[a,b]*

We report the cooperative assembly of fullerene-styrene cyano-(octyloxy)benzene triad (PCBB-CN-C8) and poly(3-hexylthiophene) (P3HT) to form the active layer of polymer solar cells (PSCs) with well-defined microstructure and enhanced stability of morphology. Favorable synergistic effect of the three functional moieties (C_{60}, styrene cyano and tri(octyloxy) chain) in PCBB-CN-C8 can not only induce P3HT to assemble into long-range ordered periodic fibrils giving interpenetrating network but also can form PCBB-CN-C8 crystallized domains without the need of external treatment. Characterization of the microstructure and morphology of P3HT:PCBB-CN-C8 blend films by two-dimensional grazing incidence X-ray diffraction, transmission electron microscope and atomic force microscopy reveals that the P3HT fibrils possess high crystallized lamellar phase, and the spacing of the periodic P3HT fibrils is approximately 10 nm depending on the PCBB-CN-C8 crystallites, which fill in the P3HT interpenetrating network. The bulk heterojunction PSCs based on P3HT:PCBB-CN-C8 exhibit an improved open-circuit voltage and excellent power conversion efficiency of 4.20%, which is greater than that of the control PSCs based on P3HT:PCBB-C8 and the devices based on P3HT:PCBM with thermal annealing. We believe that the cooperative assembly of active layer using the synergistic effect of fullerene triad is a general approach that can be used to develop external treatment-free technology, improve morphological stability of active layer and photovoltaic performance.

Introduction

Bulk heterojunction (BHJ) polymer solar cells (PSCs)[1] based on blend films of electron donating polymers with electron accepting fullerenes are receiving extensive academic and commercial interests.[2-5] The most representative PSC is based on regioregular poly(3-hexylthiophene) (P3HT) as the electron donor and [6,6]-phenyl-C_{61}-butyric acid methyl ester (PCBM) as the electron acceptor. The power conversion efficiency (PCE) of the P3HT:PCBM-based PSCs reached ca. 4% by means of thermal annealing and solvent annealing.[6, 7] Although the PCEs of the PSCs based on low band gap polymers recently surpassed 7-10%,[8-13] the P3HT donor is still very important for the application in tandem PSCs as a broad band gap polymer,[14] and in roll-to-roll fabrication of flexible large area PSCs because of its higher hole mobility.[15-17]

In developing high-performing P3HT-based PSCs, particular attention has been given to the formation of the crystallized structure of P3HT, aggregation of fullerene derivatives and the nanoscale phase-separated interpenetrating network of the active layer by external treatment methods, such as thermal annealing, mixture of solvents, additives, solvent annealing and nanoimprinting.[18-21] However, to achieve large-scale production of the PSCs on a flexible substrate like polyethylene terephthalate (PET),[22, 23] it is crucial to develop a highly reproducible fabrication procedure that can be incorporated in a roll-to-roll process, that avoids high temperature and solvent treatments to ensure compatibility with flexible substrates. Therefore, it is of great importance to develop a new approach which can achieve a well-controlled microstructure and morphology of the active layer without the need of external treatment.

Recently, we reported a tri(octyloxy)benzene-fullerene dyad (PCBB-C8)[24] with weak diffusion and aggregation ability which can induce P3HT to assemble into P3HT crystallites and nanoscale phase separation without the need of external treatment like thermal annealing or solvent annealing. The PSC based on the as-cast P3HT:PCBB-C8 blend film exhibits high short-circuit current density (J_{sc}) (8.70 mA/cm^2) which is comparable to that of a thermal annealing P3HT:PCBM device (8.87 mA/cm^2). Meanwhile, this external treatment-free technology has also been successfully applied in large area

[a] Laboratory of Advanced Optoelectronic Materials, College of Chemistry, Chemical Engineering and Materials Science, Soochow University, Suzhou 215123, China. E-mail: ywli@suda.edu.cn (Li, Y. W.); mjzhang@suda.edu.cn (Zhang, M. J.)
[b] Beijing National Laboratory for Molecular Sciences, Institution of Chemistry, Chinese Academy of Sciences, Beijing 100190, China E-mail: liyf@iccas.ac.cn (Li, Y. F.)

Electronic Supplementary Information (ESI) available: [Synthesis process of PCBB-CN-C8, ^{1}H NMR, ^{13}C NMR and MALDI-TOF spectra of PCBB-CN-C8. Electrochemical data of PCBB-Cn and PCBM; TGA thermograms; DSC of PCBB-CN-C8 and PCBM. Devices fabrication process and characterization]. See DOI: 10.1039/x0xx00000x

flexible PSCs, which presents a 1.36% PCE for a flexible PSC with a device area of 1.21 cm^2.[25] However, the diffused and weak interaction of PCBB-C8 in the self-assembly P3HT:PCBB-C8 blend film gives a low electron mobility leading to high recombination rate of photocarriers. The result is a low fill factor (*FF,* 0.49) of PSCs based on P3HT:PCBB-C8, which significantly limits further improvement of PCE of the PSCs. Furthermore, when the P3HT:PCBB-C8 blend film is treated by thermal annealing, due to the extremely low glass transition temperature (T_g, -10.7 °C) of PCBB-C8, PCBB-C8 can easily diffuse into the P3HT crystallites and result in degrading the crystallinity of P3HT. Therefore, the PCE of PSCs based on P3HT:PCBB-C8 was dramatically deteriorated after thermal annealing at 100 °C for 10 min. To overcome these drawbacks, we proposed a new concept for designing functional fullerene triad by integrating synergetic effects of fullerene triad that can induce the crystallization of P3HT and can self-assemble into stable fullerene triad.

In this work, we designed and synthesized a fullerene-styrene cyano-(octyloxy)benzene triad (PCBB-CN-C8). The [6,6]-phenyl-C_{60} is selected due to its stable fullerene skeletons and π–π stacking interaction of C_{60}. The styrene cyano bridge between fullerene and tri(octyloxy)benzene can provide electrostatic interactions, which is an important driving force for self-assembly,[26] and the van der Waals interactions of their tri(octyloxy) chain play an essential roles in inducing P3HT crystallites. When spin-coating the mixed solution of PCBB-CN-C8 and P3HT, PCBB-CN-C8 induced P3HT assemble into a highly ordered interpenetrating network with fibrillar P3HT crystallites and crystallized PCBB-CN-C8 domains under the synergistic effect of the functional PCBB-CN-C8. An excellent PCE of 4.20% was obtained by the PSCs based on P3HT:PCBB-CN-C8. The P3HT:PCBB-CN-C8 based devices also exhibited similar performances before and after thermal annealing process.

Results and discussion

The syntheitic routes and chemical structures of PCBB-CN-C8 are shown in Scheme 1, and the molecular structure of PCBB-C8 is also shown in Scheme 1 for comparison. The detailed synthetic procedure and characterizations of PCBB-CN-C8 were described in supporting information (Figure S1-3). PCBB-CN-C8 is consisted of C_{60} and tri(octyloxy) tails, which is linked by the styrene cyano bridge. It can be easily synthesized starting from commercially available chemicals, and shows good solubility in common solvents such as chloroform (CF), chlorobenzene (CB), *ortho*-dichlorobenzene (*o*-DCB), and so on due to the long tri(octyloxy) tails. The decomposition temperature (5% weight loss from thermal gravimetric analysis (TGA, in Figure S3) of PCBB-CN-C8 is at ca. 363 °C. The differential scanning calorimetry (DSC) revealed that glass transition temperatures (T_g) of PCBB-CN-C8 (T_g =32.4 °C, in Figure S4) is around the room temperature, which is much higher than that of PCBB-C8 (T_g= -10.7 °C). The increased T_g of PCBB-CN-C8 indicates that styrene cyano bridge in PCBB-CN-C8 could improve the order of tri(octyloxy) tails at room temperature.

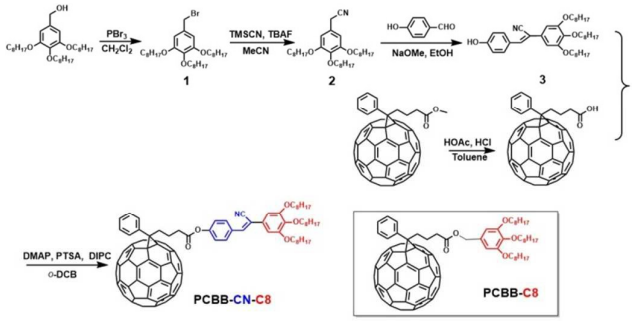

Scheme 1. Synthetic routes of PCBB-CN-C8 and molecular structure of PCBB-C8.

Figure 1(a) shows the UV-vis absorption spectra of PCBB-CN-C8, PCBB-C8 and PCBM in dilute chloroform solutions with a concentration of 10^{-5} mol/L. All the fullerene derivatives exhibit the same shape of absorption spectra with the typical feature peaks of fullerene derivative [6,6]-addition at 260 nm, 330 nm (C_{60}), and 430 nm ([6,6]-addition in C_{60}).[27] It can be clearly seen that PCBB-C8 and PCBM give the similar absorption shape and intensity,[24] while PCBB-CN-C8 shows a significant absorption enhancement both in intensity and broadth in UV region, especially at 330 nm. The peak absorption coefficients of PCBB-CN-C8, PCBB-C8 and PCBM are listed in Table 1 for a clear comparison. These results indicate that end-substitution like tri(alkoxyl)benzene tails do not affect the electronic structure of the fullerene derivatives,[24] and extending styrene cyano bridge between C_{60} and tri(alkoxyl)benzene is beneficial to enhance absorption coefficient owing to the increased conjugation of fullerene triad.

To investigate the effect of PCBB-CN-C8 triad as acceptor material on the photophysical properties of the active layer in PSCs, the UV-vis absorption spectra of the P3HT:PCBB-CN-C8, P3HT:PCBB-C8 and P3HT:PCBM blend films were measured and compared, as shown in Figure 1b. For the P3HT:PCBM blend film, the film after thermal annealing showed much more flat and red shifted peaks at around 500 nm and 554 nm (P3HT π-π* transitions), and a clearer vibronic shoulder at 604 nm (P3HT inter-chain interaction), respectively. All of these features are the typical absorption peaks for the self-assembly P3HT crystallites, which are induced by the thermal annealing process.[28, 29] In comparison, the absorption spectra of both P3HT:PCBB-CN-C8 and P3HT:PCBB-C8 blend films without thermal annealing process (as-cast) also exhibited the shape nearly identical to that of the thermal annealing P3HT:PCBM blend film, with even larger red shifts around 500 nm. These results indicate that both PCBB-CN-C8 and PCBB-C8 can induce P3HT to form crystallites by the driving force from free movable alkoxyl tails at room temperature.[24] Additionally, the as-cast P3HT:PCBB-CN-C8 blend film shows a 0.31 × 10^5 cm^{-1} absorption coefficient of P3HT, which is ca. 10% and 29% higher than those of P3HT in P3HT:PCBM with thermal annealing and as-cast P3HT:PCBB-C8, respectively, implying that P3HT crystallites induced by the PCBB-CN-C8 possessing a

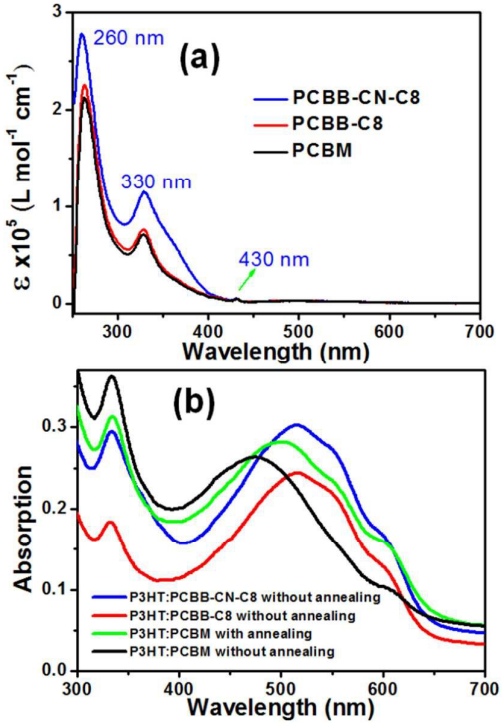

Figure 1. UV–vis absorption spectra of (a) PCBB-CN-C8, PCBB-C8 and PCBM in chloroform solutions with a concentration of 10^{-5} mol/L; (b) P3HT:PCBB-CN-C8, P3HT:PCBB-C8 and P3HT:PCBM blend films on quartz plate with or without thermal annealing.

more favorable P3HT stacking model that can utilize sunlight more efficiently than P3HT in other blend films with the same thickness.

Electrochemical cyclic voltammetry is widely used to measure the lowest unoccupied molecular orbital (LUMO) and the highest occupied molecular orbital (HOMO) energy levels of fullerene derivatives,[30] and the LUMO energy level of the fullerene derivative acceptors, which can be estimated from onset reduction potential in their cyclic voltammograms, determines the open-circuit voltage (V_{oc}) and excitons separation in BHJ PSCs.[31] **Figure 2** shows the cyclic voltammograms of PCBB-CN-C8, PCBB-C8 and PCBM films on a platinum electrode in 0.1 mol/L Bu_4NPF_6 acetonitrile solution, and the corresponding parameters are summarized in **Table 1**. The onset reduction potentials (E_{red}) of PCBB-CN-C8, PCBB-C8 and PCBM are -0.98, -0.93 and -0.94 V versus Ag/Ag^+, respectively. From the E_{red} of fullerene derivatives, their LUMO energy levels were calculated according to the equation[32] LUMO = $-e$ (E_{red} + 4.71). The LUMO energy levels of PCBB-CN-C8, PCBB-C8 and PCBM are -3.73, -3.78 and -3.77 eV, respectively. The identical LUMO energy levels of PCBB-C8 and PCBM are virtually independent of both the fullerene skeletons as well as tri(alkoxyl) chain length, which can also be confirmed by their exactly the same UV-vis absorption spectra in both shapes and intensities for the same dilute concentration in chloroform (Fig. 2a). The LUMO energy level of PCBB-CN-C8 was raised by 50-60 meV in comparison with those of PCBB-C8 and PCBM. The slight shift of LUMO level could be attributed to the extended conjugation of styrene

Table 1. The Optical and Electrochemical Data of PCBB-CN-C8, PCBB-C8 and PCBM

Fullerene derivatives	E_{red}^{onset} (V)	LUMO (eV)	Maximum absorption coefficient[a] (cm^{-1})
PCBB-CN-C8	-0.98	-3.73	0.31×10^5
PCBB-C8	-0.93	-3.78	0.28×10^5
PCBM	-0.94	-3.77	0.24×10^5

[a] The blend film of P3HT:fullerene derivative with (for PCBM) or without (for PCBB-CN-C8 and PCBB-C8) thermal annealing.

cyano bridge in PCBB-CN-C8. The effect of styrene cyano bridge on electronic structure of fullerene skeletons can also be observed from the increased and widening absorption feature peaks of [6, 6]-addition fullerene at 330 nm. The higher LUMO energy level of PCBB-CN-C8 is desirable for its application as acceptor in the PSCs with P3HT as donor to get higher V_{oc}.

To verify the cooperative self-assembly microstructures in P3HT:PCBB-CN-C8 blend films, two-dimensional grazing incidence X-ray diffraction (2D-GIXRD) is employed as a qualitative assay of the molecular packing and crystallinity of blend films, and it is particularly sensitive to the efficient assembly of P3HT.[33] The 2D-GIXRD images of P3HT:fullerene derivative blend films were shown in **Figure 3**a, and the out-of-plane GIXRD profiles extracted from the 2D-GIXRD images are provided in Figure 3b. Notable different scattering peaks for the blend films are observed. The P3HT:PCBM blend film before thermal annealing shows a diffuse and weak scattering peak around q =3.8 nm^{-1} ((100) orientation ascribing to the P3HT lamellar organized crystallites), suggesting that P3HT possesses lower crystallinity, which could be caused by the highly dispersed PCBM among the P3HT chains, and thus the restricting free regions for the crystallization of P3HT.[34, 35] After thermal annealing, the intensity of (100) diffraction peak is significantly enhanced accompanying the appearance of (200) diffraction peak, indicating a good lamellar stacking

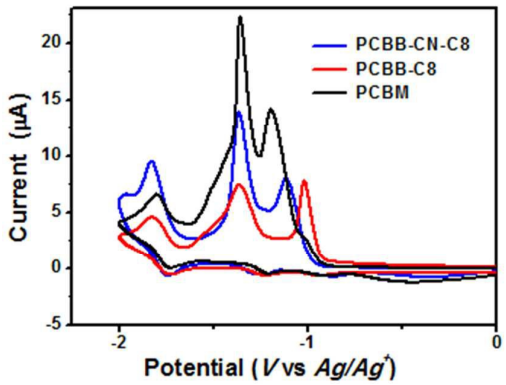

Figure 2. Cyclic voltammograms of PCBB-CN-C8, PCBB-C8 and PCBM films on platinum electrode measured in CH_3CN solution with 0.1 mol/L n-Bu_4NPF_6, at a scan rate of 100 mV/s.

Journal Name

ARTICLE

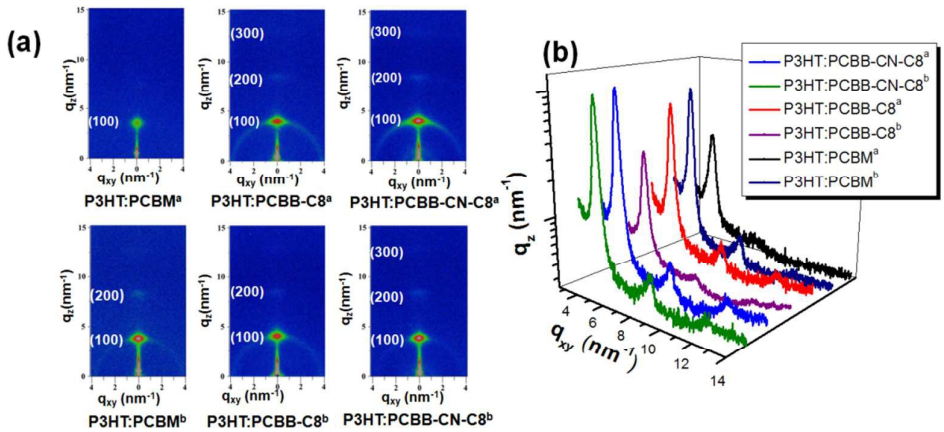

Figure 3. (a) 2D-GIXRD images of P3HT:fullerene derivative blend films with the thickness of 100 nm spin-coated from chlorobenzene or o-dichlorobenzene solution: P3HT:PCBM (w/w, 1:1), P3HT:PCBB-C8 (w/w, 1:1) and P3HT:PCBB-CN-C8 (w/w, 1:1.25); (b) out-of-plane GIXRD profiles extracted from the 2D-GIXRD images. [a] without thermal annealing; [b] with thermal annealing at 100 °C for 10 min.

order of the P3HT crystallites, which could be achieved by the driving force from thermal annealing process. Previously, we have proved that the fullerene dyad (PCBB-C8) can induce crystallization of P3HT by the driving force from flexible tri(alkoxyl) chains in PCBB-C8 during spin-coating process.[24] As shown in Figure 3a, the as-cast P3HT:PCBB-C8 blend film exhibits a higher degree of molecular order, as evidenced by the three order diffraction peaks ((100), (200), (300)) of lamellar phase. However, after thermal annealing process, the (300) diffraction peak of P3HT:PCBB-C8 blend film disappeared. This result could be explained by the weak interaction and extremely low T_g of PCBB-C8 (T_g =-10.7 °C), which can easily interpenetrate into the P3HT polymer chains and thus block the growth of P3HT crystallites under the high thermal annealing temperature. Interestingly, both the P3HT:PCBB-CN-C8 blend films with and without thermal annealing possess similar long-range ordered lamellar phase, which give (100), (200) and (300) diffraction peaks at q-values of ca. 3.8 nm^{-1}, 7.8 nm^{-1}, and 11.6 nm^{-1}, respectively, arising from the alkyl chain packing with *d*-spacing of ca. 1.65 nm. The stabilized orientation of P3HT crystallites are ascribed to the relatively high intermolecular interaction of PCBB-CN-C8, which can inhibit the PCBB-CN-C8 diffusing into P3HT polymer chains. It is worth mentioning that the above values are highly consistent with those reported for P3HT thin films,[36] indicating that alkyl side chains of P3HT are oriented vertical to the substrate to form an edge-on orientation, while the intermolecular π–π stacking between the thiophene rings is parallel to the substrate. Moreover, the intensity of (100) diffraction peak of P3HT:PCBB-CN-C8 blend films are higher than that of the other blend films, which can be observed more clearly from Figure 3b. Overall, the PCBB-CN-C8 triad with styrene cyano bridge exhibits synergistic effect on the cooperative assembly microstructures in P3HT:PCBB-CN-C8 blend films. The PCBB-CN-C8 can not only induce P3HT assembling into long-range ordered P3HT crystallites but also increase the intermolecular interaction of PCBB-CN-C8, as a consequence of stabilized molecular stacking and orientation of the two-components (P3HT and PCBB-CN-C8).

To gain deeper insight, transmission electron microscope (TEM) and atomic force microscopy (AFM) methods were used to further investigate the synergistic effect of PCBB-CN-C8 triad on cooperative assembly microstructure and morphology in P3HT:PCBB-CN-C8 blend film. While the TEM and AFM images of P3HT:PCBM and P3HT:PCBB-C8 blend films were also provided for comparison, which were shown in **Figure 4** and **Figure 5**, respectively. The insets in Figure 4 show the electron diffraction (SAED) pattern of corresponding films, revealing the crystalline order inside the film.[37] The thermal annealing P3HT:PCBM blend film shows better fibrillar P3HT crystallites than that before thermal annealing (Figure. 4a and b), which are broadly distributed in the film with an optimum morphology for high-performance BHJ PSCs.[38] A ring in the SAED pattern of as-cast P3HT:PCBM blend film (Figure 4a), corresponding to a *d*-spacing of 0.46 nm, appears weak and diffuse, which is attributed to the weak crystalline order of PCBM.[37] After thermal annealing, P3HT:PCBM blend film shows two pronounced diffraction rings. The appeared outer ring, corresponding to a *d*-spacing of 0.39 nm, is attributed to the (010) reflection of P3HT crystallites, which is associated with the typical π–π stacking distance of P3HT chains.[39] The two pronounced diffraction rings in thermal annealing P3HT:PCBM blend film indicate that both the P3HT fibrils and PCBM phase with high ordered crystallines are homogeneously

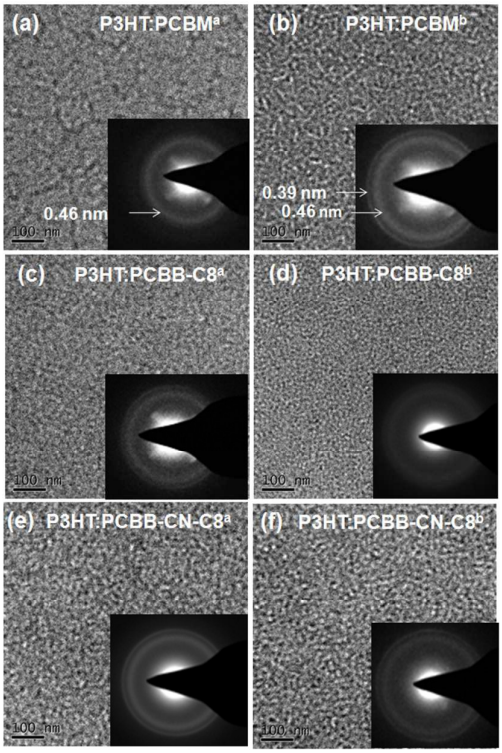

Figure 4. TEM images of P3HT:fullerene derivative blend films with the thickness of 100 nm spin-coated from CB or *o*-DCB solution: (a, b) P3HT:PCBM (w/w, 1:1); (c, d) P3HT:PCBB-C8 (w/w, 1:1); (e, f) P3HT:PCBB-CN-C8 (w/w, 1:1.25). The insets in Figure 4 are the corresponding SAED pattern. [a] without thermal annealing; [b] with thermal annealing at 100 °C for 10 min.

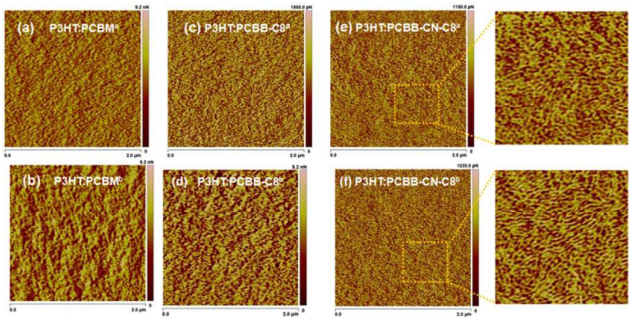

Figure 5. AFM images of P3HT:fullerene derivative blend films with the thickness of 100 nm spin-coated from CB or *o*-DCB solution: (a, b) P3HT:PCBM (w/w, 1:1); (c, d) P3HT:PCBB-C8 (w/w, 1:1); (e, f) P3HT:PCBB-CN-C8 (w/w, 1:1.25). [a] without thermal annealing; [b] with thermal annealing at 100 °C for 10 min.

dispersed throughout the film. In comparison with the thermal annealing P3HT:PCBM blend film, the as-cast P3HT:PCBB-C8 blend films also show fibrillar P3HT morphology, two diffraction rings in SAED pattern with the even same *d*-spacings (P3HT and PCBB-C8) (Figure 4c). However, the inner ring in SAED pattern of P3HT:PCBB-C8 blend film is more diffused compared with that of thermal annealing P3HT:PCBM blend film, which indicates a low crystallinity of PCBB-C8 phase. Interestingly, when processing thermal annealing, all the above crystalline features were not enhanced, but weakened (the decreased scale of fibrillar P3HT, disappeared outer ring and diffused inner ring in SAED), suggesting that the crystallites (P3HT and PCBB-C8) in P3HT:PCBB-C8 blend film was destroyed by the thermal annealing, which was consistent with the result of 2D-GIXRD. On the contrary, P3HT:PCBB-CN-C8 blend films with and without thermal annealing show a pronounced perfection of P3HT and PCBB-CN-C8 crystallites, as revealed by the high intensity of the outer and inner reflection rings, which indicates that PCBB-CN-C8 can sufficiently induce P3HT crystallites accompanying the crystallization of PCBB-CN-C8. It is noteworthy that the formed PCBB-CN-C8 crystallites can be well maintained even after thermal annealing. This result further reveals that the styrene cyano bridge in PCBB-CN-C8 can enhance the synergistic self-assembly crystallization of fullerene triad due to the increased intermolecular interaction, which can bear the high thermal annealing temperature and inhibit the diffusion of PCBB-CN-C8. More importantly, highly ordered interpenetrating network BHJ morphology of P3HT:PCBB-CN-C8 blend film has formed, evidence by the increased contrast and the appearance of bright crystallized P3HT fibrils throughout the entire film, as shown in the TEM images (Figure 4e and f). These results prove that the cooperative assembly between PCBB-CN-C8 and P3HT can form well-defined active layer via the solution spin-coating method, which avoids the external treatment like thermal or solvent annealing process.

The well-defined structure and dimensions of fibrillar P3HT crystallites in P3HT:PCBB-CN-C8 blend films can be further confirmed by the viscous force model of AFM phase images (Figure 5), which can exactly discern components by the different viscous of materials. As shown in Figure 5, the long-range ordered periodic P3HT fibrils with an approximately 10 nm spacing can only be obtained in P3HT:PCBB-C8 blend film (without thermal annealing, Figure 5c) and P3HT:PCBB-CN-C8 blend film (with and without thermal annealing, Figure 5e and f). Notably, in the case of P3HT:PCBB-CN-C8 blend films with and without thermal annealing, both films give a long fibrils (lengths of 100-180 nm, and width of approximately 12 nm), which contribute to the formation of P3HT interpenetrating network, where the PCBB-CN-C8 crystallines fill in the space between the P3HT network and form a continuous pathway for electron and hole transportation, respectively.

We studied how this cooperative assembly P3HT:PCBB-CN-C8 blend films with varying thicknesses induced by PCBB-CN-C8 triad impact the properties of photovoltaic devices. Meanwhile, the P3HT:PCBM and P3HT:PCBB-C8 based active layers were also test for comparison. The active layer in PSCs were fabricated according to the conditions of above mentioned cooperative assembly blend films, referencing the typical P3HT:PCBM active layer fabrication conditions.[29] The BHJ PSCs with a configuration of ITO/PEDOT:PSS/P3HT:fullerene derivative/Ca/Al were fabricated. **Figure 6** shows the current density-voltage (*J-V*) characteristics of the devices, and the corresponding photovoltaic parameters are given in **Table 2**. As shown in Figure 6a, the performance of PSCs based on P3HT:PCBM were improved more than 5 times after thermal annealing, which is a well known phenomenon, benefitted from highly crystallized P3HT fibrils morphology and PCBM crystallines formed during the thermal annealing. For the PSCs based on P3HT:PCBB-C8,

Journal Name

ARTICLE

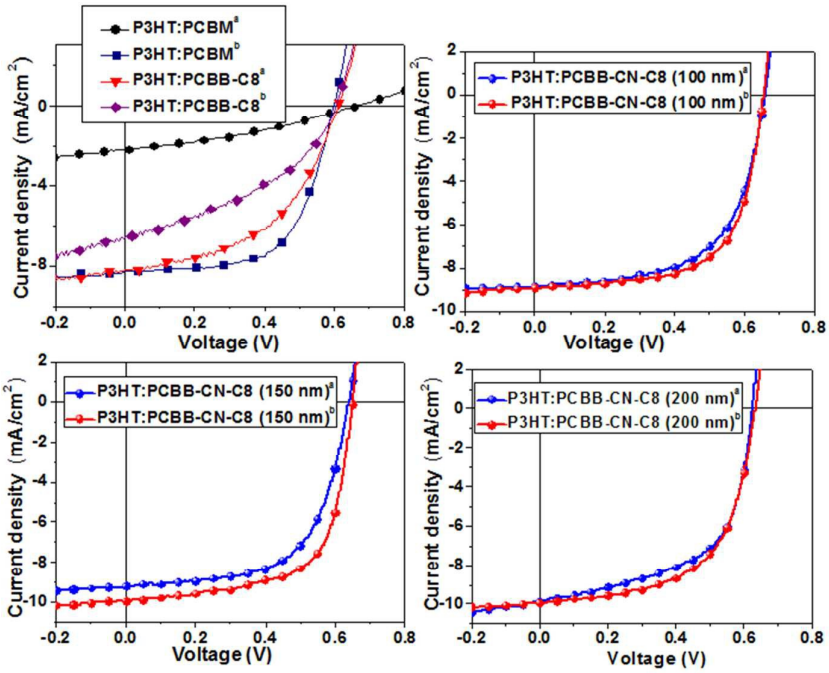

Figure 6. Current density-voltage characteristics of the PSCs based on (a) P3HT:PCBM (1:1 w/w) and P3HT:PCBB-C8 (1:1 w/w) blend film with the thickness of 100 nm spin-coated from CB solution; The P3HT:PCBB-CN-C8 (1:1.25 w/w) blend film spin-coated from *o*-DCB solution with the thickness of (b) 100 nm;. (c) 150 nm; (d) 200 nm. [a] blend film without the thermal annealing process; [b]blend film with thermal annealing at 100 °C for 10 min.

the as-prepared device without thermal annealing showed a moderate PCE of 2.61% (V_{oc} = 0.611 V, J_{sc} = 8.76 mA/cm^2 , and *FF* = 0.49) because of the formation of periodic P3HT crystallites with long-range ordered fibrils induced by PCBB-C8 during the spin-coating process. However, after thermal annealing, the PCE of the P3HT:PCBB-C8 based device dropped to 1.62%, probably due to the low glass transition temperature of PCBB-C8. Interestingly, the PSCs based on P3HT:PCBB-CN-C8 blend films (thickness of 100 nm) without thermal annealing process exhibit excellent photovoltaic performance with PCE higher than 3.51% (see Table 2). To the best of our knowledge, the PCE of higher than 3.51% is the highest photovoltaic performance among the P3HT-based PSCs without thermal annealing, which should be attributed to the well-defined microstructure and morphology of the active layer with the cooperative assembly of PCBB-CN-C8 acceptor. After thermal annealing, the photovoltaic performance of the PSCs based on P3HT:PCBB-CN-C8 was further improved, especially for the PSC with active layer thickness of 150 nm its PCE reached 4.20% after thermal annealing treatment. The excellent PCE of 4.20% is even comparable to the highest PCE of the P3HT-based PSCs reported by successive two-step (solvent and thermal annealing) treatment.[7] It should be mentioned that the thermal annealing is not so important for the PSCs based on P3HT:PCBB-CN-C8, because the as-prepared active layers in the PSCs already possess ideal donor/acceptor interpenetrating network morphology induced by the acceptor of PCBB-CN-C8. For the PSCs based on P3HT:PCBB-CN-C8 with thickness of 100 nm and 200 nm, the PCEs showed no obvious change after thermal annealing. Meanwhile, the PSCs also exhibited a stable performance after long time thermal annealing, which can be proved by the slight vibration in PCEs for the PSCs based on P3HT:PCBB-CN-C8 with thickness of 100 nm after 10 min, 30 min and 60 min thermal annealing process (as shown in Table 2).

In addition, it is also very interesting that the photovoltaic performance of the as-cast PSCs based on P3HT:PCBB-CN-C8 is almost indenpendent of the active layer thickness in the range of 100~200 nm (The PCEs are in the range of 3.50~3.60%, see Table 2). The phenomenon indicates that the crystallization of P3HT inducing by the PCBB-CN-C8 will not be affected by the solution concentration and hence the film thickness. To clarify this thickness-insensitive phenomenon, we performed the transient photovoltage (TPV) measurement to probe the photocarriers recombination dynamics in the PSCs based on as-cast P3HT:PCBB-CN-C8 with different active layer thickness of 100 nm, 150 nm and 200 nm. We also measured the devices based on as-cast P3HT:PCBB-C8 and thermal annealing

Journal Name

ARTICLE

Table 2. Characteristic Photovoltaic Parameters, Including Averages, Standard Deviations from Device under the Illumination of AM 1.5G, 100 mW/cm^2.

Active layer (thickness)	J_{sc} (mA/cm^2)	V_{oc} (V)	FF	PCE best (%)	PCE average[e] (%)	μ_h (cm^2 V^{-1}s^{-1})	μ_e (cm^2 V^{-1}s^{-1})
P3HT:PCBM[a] (100±5 nm)	2.19±0.18	0.670±0.003	0.34±0.01	0.53	0.50	5.8×10^{-4}	5.0×10^{-3}
P3HT:PCBM[b] (100±5 nm)	8.86±0.21	0.602±0.005	0.62±0.01	3.35	3.31	1.1×10^{-2}	7.8×10^{-2}
P3HT:PCBB-C8[a] (100±5 nm)	8.76±0.23	0.611±0.006	0.49±0.01	2.65	2.61	4.6×10^{-3}	1.6×10^{-2}
P3HT:PCBB-C8[b] (100±5 nm)	6.56±0.18	0.613±0.004	0.40±0.01	1.67	1.62	1.8×10^{-4}	1.4×10^{-3}
P3HT:PCBB-CN-C8[a] (100±5 nm)	8.87±0.13	0.662±0.006	0.60±0.01	3.57	3.51	8.6×10^{-3}	7.6×10^{-2}
P3HT:PCBB-CN-C8[b] (100±5 nm)	8.89±0.15	0.660±0.007	0.64±0.01	3.83	3.76	7.7×10^{-3}	6.1×10^{-2}
P3HT:PCBB-CN-C8[c] (100±5 nm)	8.52±0.13	0.660±0.004	0.63±0.01	3.57	3.51	8.6×10^{-3}	7.6×10^{-2}
P3HT:PCBB-CN-C8[d] (100±5 nm)	8.73±0.17	0.664±0.006	0.64±0.01	3.71	3.76		
P3HT:PCBB-CN-C8[a] (150±5 nm)	9.21±0.16	0.643±0.012	0.61±0.01	3.71	3.60	--	--
P3HT:PCBB-CN-C8[b] (150±5 nm)	9.95±0.19	0.651±0.009	0.65±0.01	4.26	4.20	--	--
P3HT:PCBB-CN-C8[a] (200±5 nm)	9.89±0.18	0.637±0.005	0.58±0.01	3.72	3.61	--	--
P3HT:PCBB-CN-C8[b] (200±5 nm)	9.96±0.22	0.623±0.011	0.59±0.01	3.70	3.64	--	--

[a] The active layer without thermal annealing process; [b] the active layer with thermal annealing at 100 °C for 10 min; [c] the active layer with thermal annealing at 100 °C for 30 min; [d] The active layer with thermal annealing at 100 °C for 60 min. [e] The average PCE obtained from 40 devices.

P3HT:PCBM for comparison. The details of the TPV measurement have been described elsewhere.[40] **Figure 7** shows normalized TPV curves of the devices. Briefly, devices were illuminated by white light and operated at the steady state V_{oc} condition. A small perturbed short laser pulse was used to generate extra photocarriers with a recombination lifetime of τ, as indicated by the transient decay of the photovoltage. The recombination rate (k_{rec}) of the device is therefore proportional to 1/τ. The devices based on as-cast P3HT:PCBB-CN-C8 with varying thicknesses (100 nm, 150 nm and 200 nm) show similar photovoltage decay lifetimes τ = 20.8, 20.5 and 19.7μs, respectively, which are much longer than those of the devices based on as-cast P3HT:PCBB-C8 (τ = 8.2 μs) and thermal annealing P3HT:PCBM (τ =12.9 μs). The comparable and lower recombination rates of the device based on P3HT:PCBB-CN-C8 with different thicknesses of active layers could be attributed to the similar well-defined microstructure and high charge mobilities of the active layers induced by the cooperative assembly effect of PCBB-CN-C8, which warrants that the charge carrier can be sufficiently separated in the wide range thickness of active layers to the same extent. The active layer thickness-independent photovoltaic performance is of great importance for future commercial large area production of the PSCs, in particular for the production by roll-to-roll printing.

To check the reproducibility of performance, PCEs are compared using histograms obtained from BHJ OSCs for 40 devices as shown in **Figure 8**. As can be seen from the results, all the devices exhibit high reproducibility, which generally give a standard deviation of PCEs lower than 0.04%. In addition, the independence between device performances and active layer thickness for the as-cast PSCs based on P3HT:PCBB-CN-C8 can be observed clearly from the normal distribution PCEs in Figure 8b-d (blue column). Meanwhile, as mentioned above, the slight influence of thermal annealing process on the device performance for the PSCs based on P3HT:PCBB-CN-C8 with varied thickness can also be obtained from Figure 8b-d, especially for the P3HT:PCBB-CN-C8 blend film with thickness of 200 nm, which shows almost completely overlap normal distribution area.

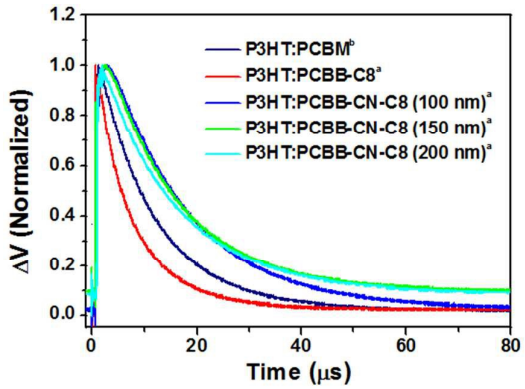

Figure 7. Normalized TPV curves of ITO/PEDOT:PSS/P3HT:PCBB-CN-C8 (or P3HT:PCBB-C8, P3HT:PCBM)/Ca/Al based solar cells under a ring of under 1W white Limited LEDs steady state background light irradiation. For the TPV the transients were induced by a low intensity, pulsed excitation (~ 20 mJ cm^{-2} excitation at 550 nm) with the device being held at either open circuit conditions.

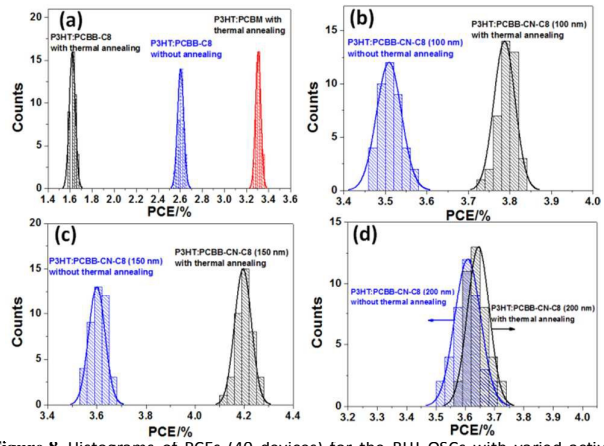

Figure 8. Histograms of PCEs (40 devices) for the BHJ OSCs with varied active layers. (a) active layers based on P3HT:PCBM and P3HT:PCBB-C8; (b) active layers based on P3HT:PCBB-CN-C8 with thickness of 100 nm; (c) active layers based on P3HT:PCBB-CN-C8 with thickness of 150 nm; (d) active layers based on P3HT:PCBB-CN-C8 with thickness of 200 nm.

All the good and high reproducibility photovoltaic results for the PSCs based on P3HT:PCBB-CN-C8 can be ascribed to the formation of bicontinuous pathways of P3HT donor with 10 nm phase separation (the higher diffraction peak intensity and three order diffraction in GIXRD, Figure 3) and higher crystallinity of PCBB-CN-C8 acceptor (high intensity of inner reflection rings in SAED, Figure 4e, f) throughout P3HT:PCBB-CN-C8 blend film. The well-defined interpenetrating network in the active layer can not only improve the hole and electron mobilities but also facilitate charge separation. It is noteworthy that although the similar morphology can also be obtained from the as-cast P3HT:PCBB-C8 blend film (Figure 5c), the relatively low crystallinity of P3HT fibrils and PCBB-C8 domain could limit the charge transportation to great extent. To give a clear explanation of the effect of the fullerene acceptors on the pbotovoltaic performance of the P3HT-based PSCs, we measured the hole and electron mobility of the blend layers of P3HT with different fullerene acceptors by the space charge limited current (SCLC) method.[41, 42] The hole mobility was measured with a hole-only device of ITO/PEDOT:PSS/P3HT:fullerene derivative/Au and estimated by the equation $J \cong (9/8)\varepsilon\varepsilon_0\mu_h V^2 \exp(0.89(V/E_0L)^{1/2})/L^3$.[43] The electron mobility was measured with an electron-only device of ITO/ poly [(9,9-bis(3′-(N,N-dimethylamino)propyl)-2,7-fluorene)-alt-2,7-(9,9-dioctylfluorene)] (PFN)/P3HT:fullerene derivative/Al and estimated by the equation $J = (8/9)\ \varepsilon_r\varepsilon_0\mu_e V^2 (V^2/L^3)$.[44] The P3HT:fullerene derivative blend film was prepared with the same method as that in the fabrication of the corresponding PSCs.

Figure 9 shows the *J*–*V* plots of different blend films, and the detailed hole and the electron mobilities (μ_e and μ_h) calculated from the plots are also listed in Table 2. The as-cast P3HT:PCBB-CN-C8 based device shows a hole mobility of 8.6×10^{-3} cm^2 V^{-1} s^{-1}, 2 times higher than that of the as-cast P3HT:PCBB-C8 based device. The obvious enhancement of hole mobility in the blend film is attributed to the increased crystallinity of P3HT fibrils induced by the PCBB-CN-C8 that improves the hole transport perpendicular to the substrate. In comparison, electron mobility of the as-cast P3HT:PCBB-CN-C8

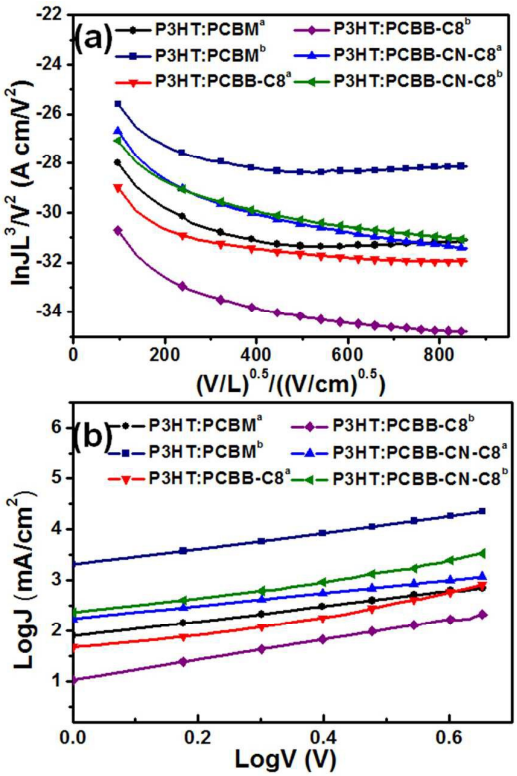

Figure 9. J–V characteristics of the (a) hole-only and (b) electron-only devices based on P3HT:fullerene derivative blend films (1:1, or 1:1.25 w/w) with the thickness of 100 nm for the measurement of hole and electron mobilities. [a] without the thermal annealing process; [b] with thermal annealing at 100 °C for 10 min.

based device (7.6×10^{-2} cm^2 V^{-1} s^{-1}) show approximately 5 times higher than that of as-cast P3HT:PCBB-C8 based device. Moreover, the P3HT:PCBB-CN-C8 based device before and after thermal annealing exhibit no obvious variation of its hole and electron mobilities. In contrast, both the hole and electron mobilities of P3HT:PCBB-C8 device are significantly deteriorated more than one order after thermal annealing. The obvious improvement in electron mobility and thermally stable charge mobility of P3HT:PCBB-CN-C8 device indicates that the incorporation of styrene cyano bridge in fullerene triad does promote the stability of self-assembly fullerene triad crystallites with high electron mobility. More importantly, the charge carrier mobility of the as-cast P3HT:PCBB-CN-C8 based device are comparable to that of the thermal annealing P3HT:PCBM device. Eventually, the remarkable and relatively balanced hole and electron transportation in P3HT:PCBB-CN-C8 blend film are helpful to restrain possible bimolecular charge recombination and improve charge collection, giving a overall enhancement of *FF* (0.58-0.65) of the corresponding PSCs compared with that of P3HT:PCBB-C8 blend film. In order to further identify the synergistic effect of PCBB-CN-C8, we select the up-to-date PTB7-Th and PDCBT as donor materials, respectively. As shown in Figure S6 and Table S1, the PTB7-Th:PCBB-CN-C8 based solar cell exhibit a disappointing performance given the low crystallization of PTB7-Th. In contrast, the performance of PDCBT:PCBB-CN-C8 based solar cell was significantly improved, which may ascribe to the

higher crystallization of PDCBT.[8] Therefore, combining the P3HT:PCBB-CN-C8 system, all above results indicate that synergistic effect of PCBB-CN-C8 is more favorable for the donor materials with high crystallization.

Conclusions

We designed and synthesized a PCBB-CN-C8 triad with room temperature T_g, which was used to induce the cooperative assembly microstructure in the active layers blended with P3HT. The synergistic effect of the three functional moieties (C60, styrene cyano and tri(octyloxy) chain) in PCBB-CN-C8 triad plays an essential role in the cooperative assembly. We found that fullerene triad can not only induce P3HT to assemble into long-range ordered periodic fibrils but also can form PCBB-CN-C8 crystallized domains without the need of external thermal treatment. This cooperative assembly microstructure consisted of bicontinuous crystallized pathways with nanoscaled phase separation is beneficial for charge separation and transportation, and shows a high hole mobility (8.6×10^{-3} cm^2 V^{-1} s^{-1}) and electron mobility (7.6×10^{-2} cm^2 V^{-1} s^{-1}), which are comparable to those of thermal annealing P3HT:PCBM blend film. We fabricated the BHJ PSCs by using this cooperative assembly P3HT:PCBB-CN-C8 blend film as active layer, and found that the PSCs demonstrated thermal stable and active-layer-independent photovoltaic performance in the thickness range of 100~200 nm. The best PCE of 4.20% was achieved for the PSC based on P3HT:PCBB-CN-C8 with active-layer-thickness of 150 nm and thermal annealing at 100 ^{o}C for 10 min, which is higher than the PCE (3.31%) of the PSCs based on thermal annealing P3HT:PCBM. Given the synergistic effect of fullerene triad and the high crystallinity of P3HT, this strategy can be used to develop efficient external treatment-free PSCs by a rational design of fullerene triad and selection of donor materials.

Acknowledgements

This work was supported by the National Natural Science Foundation of China (Grant No. 21204057, 91333204, 51422306), and Jiangsu Provincial Natural Science Foundation (Grant No. BK2012213). Priority Academic Program Development of Jiangsu Higher Education Institutions.

Notes and references

1. G. Yu, J. Gao, J. C. Hummelen, F. Wudl and A. J. Heeger, *Science*, 1995, **270**, 1789-1791.
2. G. Li, R. Zhu and Y. Yang, *Nat Photon*, 2012, **6**, 153-161.
3. Y. Li, *Accounts of Chemical Research*, 2012, **45**, 723-733.
4. z. Zhang and Y. Li, *Science China Chemistry*, 2015, **58**, 192-209.
5. S. Zhang, L. Ye, W. Zhao, B. Yang, Q. Wang and J. hou, *Science China Chemistry*, 2015, **58**, 248-256.
6. P. Schilinsky, C. Waldauf and C. J. Brabec, *Appl Phys Lett*, 2002, **81**, 3885-3887.
7. G. Li, V. Shrotriya, J. Huang, Y. Yao, T. Moriarty, K. Emery and Y. Yang, *Nature Materials*, 2005, **4**, 864-868.
8. M. Zhang, X. Guo, W. Ma, H. Ade and J. Hou, *Advanced Materials*, 2014, **26**, 5880-5885.
9. C. Cui, W.-Y. Wong and Y. Li, *Energy & Environmental Science*, 2014, **7**, 2276-2284.
10. Z. He, B. Xiao, F. Liu, H. Wu, Y. Yang, S. Xiao, C. Wang, T. P. Russell and Y. Cao, *Nat Photon*, 2015, **9**, 174-179.
11. Y. Liu, J. Zhao, Z. Li, C. Mu, W. Ma, H. Hu, K. Jiang, H. Lin, H. Ade and H. Yan, *Nat Commun*, 2014, **5**, 5293.
12. I. Etxebarria, A. Guerrero, J. Albero, G. Garcia-Belmonte, E. Palomares and R. Pacios, *Organic Electronics*, 2014, **15**, 2756-2762.
13. Y. Yang, W. Chen, L. Dou, W.-H. Chang, H.-S. Duan, B. Bob, G. Li and Y. Yang, *Nat Photon*, 2015, **9**, 190-198.
14. J. You, L. Dou, K. Yoshimura, T. Kato, K. Ohya, T. Moriarty, K. Emery, C.-C. Chen, J. Gao, G. Li and Y. Yang, *Nat Commun*, 2013, **4**, 1446.
15. Z. Bao, A. Dodabalapur and A. J. Lovinger, *Appl Phys Lett*, 1996, **69**, 4108-4110.
16. N. Espinosa, M. Hosel, D. Angmo and F. C. Krebs, *Energy & Environmental Science*, 2012, **5**, 5117-5132.
17. S. Choi, Y. Zhou, W. Haske, J. W. Shim, C. Fuentes-Hernandez and B. Kippelen, *Organic Electronics*, 2015, **17**, 349-354.
18. N. Seidler, G. M. Lazzerini, G. Li Destri, G. Marletta and F. Cacialli, *Journal of Materials Chemistry C*, 2013, **1**, 7748-7757.
19. D. Chen, F. Liu, C. Wang, A. Nakahara and T. P. Russell, *Nano letters*, 2011, **11**, 2071-2078.
20. X. Guo, C. Cui, M. Zhang, L. Huo, Y. Huang, J. Hou and Y. Li, *Energy & Environmental Science*, 2012, **5**, 7943-7949.
21. G. Ding, C. Li, X. Li, Y. Wu, J. Liu, Y. Li, Z. Hu and Y. Li, *Nanoscale*, 2015, **7**, 11024-11032.
22. G. D. Spyropoulos, P. Kubis, N. Li, D. Baran, L. Lucera, M. Salvador, T. Ameri, M. M. Voigt, F. C. Krebs and C. J. Brabec, *Energy & Environmental Science*, 2014, **7**, 3284-3290.
23. L. Mao, Q. Chen, Y. Li, Y. Li, J. Cai, W. Su, S. Bai, Y. Jin, C.-Q. Ma, Z. Cui and L. Chen, *Nano Energy*, 2014, **10**, 259-267.
24. P. Zhang, C. Li, Y. Li, X. Yang, L. Chen, B. Xu, W. Tian and Y. Tu, *Chemical Communications*, 2013, **49**, 4917-4919.
25. Y. Li, L. Mao, Y. Gao, P. Zhang, C. Li, C. Ma, Y. Tu, Z. Cui and L. Chen, *Solar Energy Materials and Solar Cells*, 2013, **113**, 85-89.
26. C. J. Takacs, Y. Sun, G. C. Welch, L. A. Perez, X. Liu, W. Wen, G. C. Bazan and A. J. Heeger, *Journal of the American Chemical Society*, 2012, **134**, 16597-16606.
27. J. C. Hummelen, B. W. Knight, F. LePeq, F. Wudl, J. Yao and C. L. Wilkins, *The Journal of Organic Chemistry*, 1995, **60**, 532-538.
28. J. Jo, S.-S. Kim, S.-I. Na, B.-K. Yu and D.-Y. Kim, *Advanced Functional Materials*, 2009, **19**, 866-874.
29. W. Ma, C. Yang, X. Gong, K. Lee and A. J. Heeger, *Advanced Functional Materials*, 2005, **15**, 1617-1622.
30. Y. He, H.-Y. Chen, J. Hou and Y. Li, *Journal of the American Chemical Society*, 2010, **132**, 1377-1382.
31. C. J. Brabec, A. Cravino, D. Meissner, N. S. Sariciftci, T. Fromherz, M. T. Rispens, L. Sanchez and J. C. Hummelen, *Advanced Functional Materials*, 2001, **11**, 374-380.
32. Q. Sun, H. Wang, C. Yang and Y. Li, *Journal of Materials Chemistry*, 2003, **13**, 800-806.

33. F. Li, K. G. Yager, N. M. Dawson, Y.-B. Jiang, K. J. Malloy and Y. Qin, *Chemistry of Materials*, 2014, **26**, 3747-3756.
34. B. C. Thompson and J. M. J. Fréchet, *Angewandte Chemie International Edition*, 2008, **47**, 58-77.
35. P. M. Beaujuge and J. M. J. Fréchet, *Journal of the American Chemical Society*, 2011, **133**, 20009-20029.
36. T.-A. Chen, X. Wu and R. D. Rieke, *Journal of the American Chemical Society*, 1995, **117**, 233-244.
37. X. Yang, J. K. J. van Duren, M. T. Rispens, J. C. Hummelen, R. A. J. Janssen, M. A. J. Michels and J. Loos, *Advanced Materials*, 2004, **16**, 802-806.
38. X. Yang, J. Loos, S. C. Veenstra, W. J. H. Verhees, M. M. Wienk, J. M. Kroon, M. A. J. Michels and R. A. J. Janssen, *NANO LETTERS*, 2005, **5**, 579-583.
39. K. J. Ihn, J. Moulton and P. Smith, *Journal of Polymer Science Part B: Polymer Physics*, 1993, **31**, 735-742.
40. Y.-Y. Lin, T.-H. Chu, S.-S. Li, C.-H. Chuang, C.-H. Chang, W.-F. Su, C.-P. Chang, M.-W. Chu and C.-W. Chen, *Journal of the American Chemical Society*, 2009, **131**, 3644-3649.
41. G. G. Malliaras, J. R. Salem, P. J. Brock and C. Scott, *Physical Review B*, 1998, **58**, R13411-R13414.
42. V. R. Nikitenko, H. Heil and H. von Seggern, *Journal of Applied Physics*, 2003, **94**, 2480-2485.
43. C. Li, Y. Chen, Y. Zhao, H. Wang, W. Zhang, Y. Li, X. Yang, C. Ma, L. Chen, X. Zhu and Y. Tu, *Nanoscale*, 2013, **5**, 9536-9540.
44. X. Guo, M. Zhang, C. Cui, J. Hou and Y. Li, *Acs Applied Materials & Interfaces*, 2014, **6**, 8190-8198.

Yue Zhao,[a] Guiying Xu,[a] Xia Guo,[a] Yijun Xia,[a]

Chaohua Cui,[a] Maojie Zhang,[a] Bo Song,[a] Yaowen*

Li,[a] Yongfang Li*[a,b]*

Journal of Materials Chemistry A

Title: Cooperative Assembly of Active Layer Utilizing the Synergistic Effect of Functional Fullerene Triad as Acceptor for Efficient and Thermally Stable P3HT-based Polymer Solar Cells

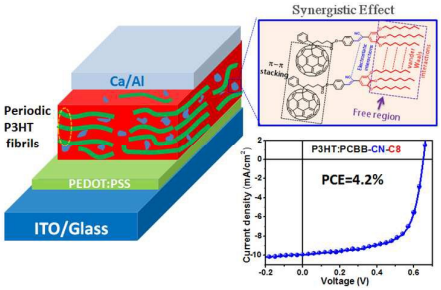

In this manuscript, we firstly reported a fullerene-styrene cyano-(octyloxy)benzene triad (PCBB-CN-C8) as acceptor materials, which can cooperative assemble with poly(3-hexylthiophene) (P3HT) to form the active layer of polymer solar cells (PSCs) with well-defined microstructure and enhanced stability of morphology (without external treatment like thermal annealing or solvent annealing). The bulk heterojunction (BHJ) PSCs based on P3HT:PCBB-CN-C8 exhibit overall improved photovoltaic performance including improved open-circuit voltage, thickness-independent and excellent power conversion efficiency (PCE). The PSC based on as-cast P3HT:PCBB-CN-C8 exhibit a PCE of higher than 3.60%, which is the highest photovoltaic performance among the P3HT-based PSCs without thermal annealing. The PCE of 4.20% after thermal annealing is comparable to the highest reported PCE of the P3HT-based PSCs by successive two-step (solvent and thermal annealing) treatment.